

## Gating orbital memory with an atomic donor

Elze J. Knol<sup>1</sup>, Brian Kiraly<sup>1</sup>, Alexander N. Rudenko<sup>1,2</sup>, Werner M. J. van Weerdenburg<sup>1</sup>, Mikhail I. Katsnelson<sup>1,2</sup>, Alexander A. Khajetoorians<sup>1</sup>

1. *Institute for Molecules and Materials, Radboud University, Nijmegen 6525AJ, The Netherlands*
2. *Theoretical Physics and Applied Mathematics Department, Ural Federal University, 620002 Ekaterinburg, Russia*

**Orbital memory is defined by two stable valencies that can be electrically switched and read-out. To explore the influence of an electric field on orbital memory, we studied the distance-dependent influence of an atomic Cu donor on the state favorability of an individual Co atom on black phosphorus. Using low temperature scanning tunneling microscopy/spectroscopy, we characterized the electronic properties of individual Cu donors, corroborating this behavior with *ab initio* calculations based on density functional theory. We studied the influence of an individual donor on the charging energy and stochastic behavior of an individual Co atom. We found a strong impact on the state favorability in the stochastic limit. These findings provide quantitative information about the influence of local electric fields on atomic orbital memory.**

A single magnetic atom on a surface can exhibit multiple valencies, as predicted for various  $3d$  transition metal atoms on the surface of graphene [1, 2]. This concept was experimentally demonstrated, using scanning tunneling microscopy/spectroscopy (STM/STS), with individual Co atoms on the surface of semiconducting black phosphorus (BP) [3]. In this study, the two stable valencies of an individual Co atom residing in a hollow site were observed via their different charge densities, and could be switched electrically, serving as a so-called orbital memory. Moreover, the electric field generated by the probe could be used to ionize an individual Co atom, leading to stochastic fluctuations between the stable configurations characterized by telegraph noise in the tunneling current. It was later shown that the stochastic behavior of arrays of coupled orbital memories exhibits tunable multiplicity, a precursor to glassy dynamics characteristic in multi-well systems [4-6]. In this way, arrays of orbital memories are a promising platform to mimic machine learning at the atomic scale, due to their long-range connectivity and competing interactions.

Understanding the influence of an electric field on orbital memory is vital both fundamentally as well as for its utility, in analogy to the effect of a magnetic field on spin-based memory [7-9]. One way to quantify the role of an electric field on the bistable valency is to place well-defined atomic-scale dopants near individual orbital memories, and probe the response of the bistable valency. In this vain, it has been shown that alkali atoms are charge donors on the surface of BP. For instance, it was shown that K atoms can be used to *n*-dope BP [10-12] and probe the anisotropic dielectric screening of the material [13]. However, K atoms are relatively challenging to use for STM-based studies, as they easily diffuse on the surface of BP and can be laterally perturbed by the tip-generated electric field.

Here, we explore the influence of a single donor, derived from an individual Cu atom, on the bistable valency of an isolated Co atom on BP. Using STM/STS, we probe changes in the ionization energy of individual Co atoms in proximity to single Cu-type donors, using atomic scale manipulation. We quantify and correlate these changes with the modified stochastic switching of individual Co atoms in proximity to Cu donors. We observe a strong change in the state dependent lifetime of the Co atom, depending on the separation between the Co and Cu species. Using first principles calculations based

on density functional theory (DFT), we find that each valency exhibits a unique electric dipole moment, leading to a substantially different response to the local electric field generated by the Cu donor.

STM and STS measurements were performed with a commercial Omicron low-temperature STM in ultrahigh vacuum ( $p = < 1 \times 10^{-10}$  mbar) and at a base temperature of  $T = 4.4$  K. The bias was applied to the sample ( $V_s$ ). All measurements were performed with electrochemically etched W tips. The tips were treated *in situ* by electron bombardment and field emission, whereafter they were dipped and characterized on a clean Au(111) surface. The STM images in this work were all acquired using constant-current feedback. STS measurements were performed using a lock-in technique to directly measure  $dI/dV$ . A modulation was applied to the bias signal of  $V_{mod} = 6$  mV at a frequency of  $f_{mod} = 817.7$  Hz. All telegraph measurements were acquired with the tip at constant height. The tip height was stabilized with constant-current feedback on the bare BP at  $I = 20$  pA,  $V_s = -400$  mV, before opening the feedback loop. BP crystals were purchased from HQ graphene. The crystals were cleaved with scotch tape in UHV and immediately transferred to the microscope for *in situ* characterization. Co and Cu were evaporated cold directly into microscope with during the dosing procedure. Atomic manipulation of the Co atoms was performed by dragging the top-site atoms along the [010] direction in constant-current mode with  $-130$  mV  $< V_s < -100$  mV and  $6$  nA  $< I_t < 12$  nA. After a Co atom reached a desirable location (with respect to a Cu species), it was manipulated into a hollow site by means of a voltage pulse of  $V_s < -700$  mV.

DFT calculations were carried out using the projected augmented-wave method (PAW) [14] as implemented in the Vienna *ab initio* simulation package (VASP) [15, 16]. Exchange and correlation effects were taken into account within the spin-polarized generalized gradient approximation (GGA-PBE) [17]. The Hubbard-U correction was not applied to Cu atoms because the 3d shell of Cu is almost entirely filled and, therefore, is not sensitive to additional local Coulomb interaction. An energy cutoff of 300 eV for the plane-wave basis and the convergence threshold of  $10^{-6}$  eV were used, which is sufficient to obtain numerical accuracy. Pseudopotentials were taken to include 3s and 3p valence electrons for P atom, as well as 3d and 4s valence electrons for Cu atoms. The BP surface was modeled in the slab geometry by a single BP layer with dimensions  $(3a \times 4b) \approx (13.1 \times 13.3)$  Å with

atomic positions fixed to the experimental parameters of bulk BP [18]. Vertical separation between the layers was set to 20 Å. The Brillouin zone was sampled by a uniform distribution of  $\mathbf{k}$ -points on a (8 × 8) mesh. The position of the Cu atom was relaxed considering top and hollow surface sites as starting points. The projection of the electronic bands on specific atomic states was performed using the formalism of Wannier functions [19] implemented in the wannier90 package [20]. The charge transfer from Cu to BP,  $\Delta n$ , was estimated as a difference between the number of Cu valence electrons in a free atom ( $N=11$ ) and in the atom adsorbed on BP ( $n$ ), that is  $\Delta n = N - n$ , where  $n$  is calculated by integrating the density of states  $g(E)$  projected onto the s- and d-orbitals of Cu,  $n = \int_{-\infty}^{E_F} g(E)dE$  with  $E_F$  being the Fermi energy. The electric dipole moment at finite electric fields was calculated from the vertical distribution of the charge density  $n(z) = \frac{1}{S} \int n(\mathbf{r})dxdy$  by applying a saw-tooth potential in the direction normal to the BP surface. The calculations for a Co adatom on BP were performed for two orbital configurations (low-spin and high-spin) using the same parameters as in ref [3].

Fig. 1(a) illustrates an STM image of a cleaved BP surface after deposition of Co and Cu atoms. In agreement with previous experiments [3, 21], intrinsic vacancies are identified as elongated dumbbell-shaped protrusions with varying intensity, depending on their depth. An individual Co atom preferentially adsorbs onto a top site, and its charge density can be identified as a bi-lobed, butterfly-like shape. The Co atom can be manipulated into a hollow site, using the STM tip, as described in ref [3]. In constant-current STM imaging, Co atoms residing in a hollow site can exhibit two different charge densities ( $\text{Co}_{\text{high}}$  and  $\text{Co}_{\text{low}}$ ). These two unique charge densities result from the bistable valency of the Co atom, as described in ref [3], and these two states can be reversibly switched with a voltage pulse.

Cu atoms can be differentiated from Co atoms due to their distinguishable charge densities in constant-current imaging. Three different Cu species were observed, all characterized by an ellipse-shaped outer depression whereas the internal pattern is distinct between all three species. Fig. 1(b-d) show detailed images of the appearance of each of these species. Based on a binding site analysis comparing the charge density in constant-current imaging with the underlying BP lattice and *ab initio* calculations of the relaxed charge density (discussed below), we find that two of the species reside in

a hollow site, and one species resides on a top site. Both hollow site species are identified as isotropic protrusions and can be distinguished by the presence/absence of a circular depression directly around the center of this protrusion and distinct apparent heights of  $13 \pm 1$  pm /  $97 \pm 2$  pm at  $V_s = -400$  mV for the species in Fig. 1 (b) and (c) respectively. The Cu atoms residing in the top site ( $Cu_T$ ) are identified by their bi-lobed shapes and an apparent height of  $52 \pm 4$  pm at  $V_s = -400$  mV. Two types of these top site atoms are observed, related through mirror symmetry along the zig-zag [010] direction (Supplementary Fig. 1). While both hollow site species can potentially be attributed to bistable valency, like for Co, we subsequently show that the difference between both Cu atoms at the hollow site results from hydrogen adsorption (see Supplementary Fig. 1) [22-26]. After deposition at  $T < 5$  K,  $\sim 68\%$  of the Cu atoms reside in a hollow site and  $\sim 32\%$  reside on a top site. The amount of hydrogenated hollow site species increased over time.

In order to quantify the electronic properties of each Cu species and relate this to the experimental observations, we performed DFT calculations for a Cu atom on BP surface. We calculated the band structure of Cu atoms residing in the hollow and top site (see Supplementary Fig. 3) on BP, as well as of hydrogenated Cu in the hollow site ( $CuH_H$ ). In case of Cu and CuH residing in the hollow site, the system is nonmagnetic, whereas a small magnetic moment of  $\sim 0.5 \mu_B$  appears for Cu in the top site. We also calculated the spatial distribution of the charge densities projected on the valence states of BP (Fig. 1(e-g)), which can be directly associated with the STM images (Fig. 1(b-d)). Based on these calculations, we conclude that the experimentally observed species in Fig. 1(b) and Fig. 1(d) are the hollow and top site, respectively. We also considered CuH species, and confirm that charge density observed in Fig. 1(c) coincides with  $CuH_H$ . From DFT calculations follows that  $Cu_H$  species donate 0.7 electrons to the BP substrate,  $CuH_H$  species donate 0.12 electrons and  $Cu_T$  species donate 0.24 electrons. The electrons are mostly donated from the 4s shell of Cu, whereas the 3d shell remains fully occupied. These calculations are consistent with experimental observations of *n*-doping at higher Cu coverages (see Supplementary Fig. 2). Therefore, we consider all Cu species as donors in the subsequent discussion, which is line with previous literature [27-30]. In the following experiments, a relatively low areal density of  $n_{Cu} = 0.165 \times 10^{12} \text{ cm}^{-2}$  was used to ensure minimal band shifts in the BP ( $< 8$  meV).

In order to probe the influence of Cu donors on the bistable valency of individual Co atoms, we first studied the response of the  $\text{Co}_{\text{low}}$  atom charging peak as a function of distance ( $r$ ) from a single, isolated Cu atom. As shown in ref [3], Co impurity states near  $E_F$  can be pulled above the  $E_F$ , via tip-induced band bending [31-33]. This leads to a peak in STS near  $V_S = 370$  mV, which depends on the tip and tunneling conditions). We observed that this charging peak shifts to higher energy ( $\Delta V = 118$  mV, defined with respect to the peak energy of an isolated atom,  $\Delta V = V(r) - V(r > 10 \text{ nm})$ ) when the Co atom is near  $\text{CuH}_\text{H}$  ( $r = 3.8 \text{ nm}$ ) (Fig. 2). We attribute this change in the relative charging peak energy to local downward band bending from  $\text{CuH}_\text{H}$  [34, 35], which acts concomitantly with tip-induced band bending on the Co atom. To overcome the downward band bending from the  $\text{CuH}_\text{H}$ , more tip-induced band bending is required to ionize the Co atom, thus the ionization peak is observed at a higher energy.

In order to quantify the influence of the Cu donor, we measured the charging peak shift  $\Delta V(r)$  at various values of  $r$  and for the three different Cu species (Fig. 3). (See Supplementary Fig. 4 for the absolute peak energies  $V(r)$ .) The studied Co-Cu pairs were created utilizing atomic manipulation of Co atoms. At distances  $r > 10 \text{ nm}$ , there is no shift of the ionization energy, i.e.  $\Delta V$  is negligible. At smaller distances,  $\Delta V$  increases monotonically. This is indicative of the influence of surface-induced band bending derived from the Cu species, which depends on the substrate-driven dielectric screening of the potential energy generated by the Cu species. The results in Fig. 3 include  $\text{Co-Cu}_\text{T}$ ,  $\text{Co-Cu}_\text{H}$  and  $\text{Co-CuH}_\text{H}$  pairs in both orientations with respect to the mirror-symmetry in the [100] direction and various directions (most pairs were built roughly along the [100] and [010] directions). This indicates that the band bending profiles are similar for all Cu species and insensitive to the relative orientation between the atomic displacement vector and the lattice vectors ( $r$ ) of the BP.

To understand the influence of a local electric field on orbital memory, we studied the influence of a Cu-based donor on the stochastic noise of a nearby Co atom as a function of  $r$  (Fig. 4). By applying voltages typically above  $V_S > 400$  mV, isolated Co atoms exhibit telegraph noise resulting from stochastic switching between the bistable valencies:  $\text{Co}_{\text{high}}$  and  $\text{Co}_{\text{low}}$  (Fig. 4 (a)) [3]. We subsequently

measured the telegraph noise of a Co atom, within the proximity of a Cu species. We measured the telegraph noise until we approach steady state (typically  $\sim$ 800 switching events), in order to be able to extract the state dependent lifetime ( $\tau_{\text{high}}$  and  $\tau_{\text{low}}$ ), as done in refs [3, 36]. We extracted  $\tau_{\text{high}}$  and  $\tau_{\text{low}}$  for multiple tips and atoms, with varying values of  $r$  (Fig. 4 (b-c)) at two sample biases ( $V_s = 500$  and  $550$  mV). As in Fig. 3, the results in Fig. 4 (b-c) include Co-Cu<sub>T</sub>, Co-Cu<sub>H</sub> and Co-CuH<sub>H</sub> pairs in various orientations and directions. The most striking feature is that the lifetime of the Co<sub>high</sub> state ( $\tau_{\text{high}}$ ) is dramatically decreased by the proximity of the Cu donor, whereas the Co<sub>low</sub> state is only weakly perturbed in comparison. At  $V_s = 500$  mV, lifetime  $\tau_{\text{high}}$  decreases from approximately 170 ms to 30 ms for decreasing  $r$  from  $\sim$ 16 to 4 nm and at  $V_s = 550$  mV,  $\tau_{\text{high}}$  decreases more than an order of magnitude, from roughly 70 ms to 5 ms. This observation implies that Co<sub>high</sub> state has a significant electric dipole moment, which is strongly influenced by the electric field emanating from the nearby Cu species. DFT calculations reveal that the Co<sub>low</sub> and Co<sub>high</sub> states of the Co atom both have an electric dipole moment perpendicular to the BP surface:  $d_{\text{low}} = -0.12$  eÅ and  $d_{\text{high}} = -0.22$  eÅ (without an external electric field, see Supplementary Fig. 5). Next to the presence of an electric dipole moment, the observation that only Co<sub>high</sub> is affected may also be related to the difference in dielectric screening induced by the substrate: the screening of the Co<sub>high</sub> state by the substrate is weaker with respect to the Co<sub>low</sub> state, as was demonstrated in ref [3].

In conclusion, we demonstrated the effect of a controlled electric field generated by an individual Cu donor on the atomic orbital memory of Co on BP. Using both STM/STS and DFT calculations, we quantified the distance-dependent influence of individual Cu donors on the ionization energy of Co, as well as on the state-dependent lifetime in the stochastic limit. The monotonous increase in the charging energy of Co<sub>low</sub> with decreasing  $r$  maps the downward band bending associated with the single Cu atoms. We also find that the proximity to local donors strongly influences the Co<sub>high</sub> state, whereas there is no influence on the Co<sub>low</sub> state. This gives experimental evidence of a strong electric dipole moment in the Co<sub>high</sub> state, which was confirmed by DFT calculations. Notably, we detected no difference in the effect of the different Cu species on the ionization energy or stochastic behavior of Co. Our findings illustrate how the state favorability of an atomic orbital memory, i.e. the energy landscape, can be tuned by an external electric field, analogous to a magnetic field in a spin-based

memory. It remains to be seen how the spin states and crystal field are locally affected by the presence of the electric field.

### Acknowledgements

The experimental part of this project was supported by the European Research Council (ERC) under the European Union's Horizon 2020 research and innovation programme (grant no. 818399). E. J. K. and A. A. K. acknowledge support from the NWO-VIDI project 'Manipulating the interplay between superconductivity and chiral magnetism at the single-atom level' with project no. 680-47-534. B. K. acknowledges the NWO-VENI project 'Controlling magnetism of single atoms on black phosphorus' with project no. 016.Veni.192.168. For the theoretical part of this work, A. N. R. and M. I. K. received funding from the European Research Council via Synergy Grant 854843 – FASTCORR.

### References

1. T. O. Wehling, A. I. Lichtenstein and M. I. Katsnelson, *Physical Review B* **84** (23), 235110 (2011).
2. A. N. Rudenko, F. J. Keil, M. I. Katsnelson and A. I. Lichtenstein, *Physical Review B* **86** (7), 075422 (2012).
3. B. Kiraly, A. N. Rudenko, W. M. J. van Weerdenburg, D. Wegner, M. I. Katsnelson and A. A. Khajetoorians, *Nature Communications* **9** (1), 3904 (2018).
4. A. Kolmus, M. I. Katsnelson, A. A. Khajetoorians and H. J. Kappen, *New Journal of Physics* **22** (2), 023038 (2020).
5. U. Kamber, A. Bergman, A. Eich, D. İlşan, M. Steinbrecher, N. Hauptmann, L. Nordström, M. I. Katsnelson, D. Wegner, O. Eriksson and A. A. Khajetoorians, *Science* **368** (6494), eaay6757 (2020).
6. B. Kiraly, E. J. Knol, W. M. J. van Weerdenburg, H. J. Kappen and A. A. Khajetoorians, *Nature Nanotechnology* **16** (4), 414-420 (2021).
7. F. Donati, S. Rusponi, S. Stepanow, C. Wäckerlin, A. Singha, L. Persichetti, R. Baltic, K. Diller, F. Patthey, E. Fernandes, J. Dreiser, Ž. Šljivančanin, K. Kummer, C. Nistor, P. Gambardella and H. Brune, *Science* **352** (6283), 318 (2016).
8. F. E. Kalff, M. P. Rebergen, E. Fahrenfort, J. Girovsky, R. Toskovic, J. L. Lado, J. Fernández-Rossier and A. F. Otte, *Nature Nanotechnology* **11** (11), 926-929 (2016).
9. F. D. Natterer, K. Yang, W. Paul, P. Willke, T. Choi, T. Greber, A. J. Heinrich and C. P. Lutz, *Nature* **543** (7644), 226-228 (2017).
10. J. Kim, S. S. Baik, S. H. Ryu, Y. Sohn, S. Park, B.-G. Park, J. Denlinger, Y. Yi, H. J. Choi and K. S. Kim, *Science* **349** (6249), 723 (2015).
11. S.-W. Kim, H. Jung, H.-J. Kim, J.-H. Choi, S.-H. Wei and J.-H. Cho, *Physical Review B* **96** (7), 075416 (2017).
12. C. Han, Z. Hu, L. C. Gomes, Y. Bao, A. Carvalho, S. J. R. Tan, B. Lei, D. Xiang, J. Wu, D. Qi, L. Wang, F. Huo, W. Huang, K. P. Loh and W. Chen, *Nano Letters* **17** (7), 4122-4129 (2017).
13. B. Kiraly, E. J. Knol, K. Volckaert, D. Biswas, A. N. Rudenko, D. A. Prishchenko, V. G. Mazurenko, M. I. Katsnelson, P. Hofmann, D. Wegner and A. A. Khajetoorians, *Physical Review Letters* **123** (21), 216403 (2019).
14. P. E. Blochl, *Physical Review B* **50** (24), 17953-17979 (1994).
15. G. Kresse and J. Furthmüller, *Physical Review B* **54** (16), 11169-11186 (1996).
16. G. Kresse and D. Joubert, *Physical Review B* **59** (3), 1758-1775 (1999).
17. J. P. Perdew, K. Burke and M. Ernzerhof, *Physical Review Letters* **77** (18), 3865-3868 (1996).

18. A. Brown and S. Rundqvist, *Acta Crystallographica* **19** (4), 684-685 (1965).
19. N. Marzari, A. A. Mostofi, J. R. Yates, I. Souza and D. Vanderbilt, *Reviews of Modern Physics* **84** (4), 1419-1475 (2012).
20. A. A. Mostofi, J. R. Yates, Y.-S. Lee, I. Souza, D. Vanderbilt and N. Marzari, *Computer Physics Communications* **178** (9), 685-699 (2008).
21. B. Kiraly, N. Hauptmann, A. N. Rudenko, M. I. Katsnelson and A. A. Khajetoorians, *Nano Letters* **17** (6), 3607-3612 (2017).
22. A. Zhao, Q. Li, L. Chen, H. Xiang, W. Wang, S. Pan, B. Wang, X. Xiao, J. Yang, J. G. Hou and Q. Zhu, *Science* **309** (5740), 1542 (2005).
23. N. Baadji, S. Kuck, J. Brede, G. Hoffmann, R. Wiesendanger and S. Sanvito, *Physical Review B* **82** (11), 115447 (2010).
24. B. W. Heinrich, G. Ahmadi, V. L. Müller, L. Braun, J. I. Pascual and K. J. Franke, *Nano Letters* **13** (10), 4840-4843 (2013).
25. A. A. Khajetoorians, T. Schlenk, B. Schweflinghaus, M. dos Santos Dias, M. Steinbrecher, M. Bouhassoune, S. Lounis, J. Wiebe and R. Wiesendanger, *Physical Review Letters* **111** (15), 157204 (2013).
26. V. C. Zoldan, R. Faccio and A. A. Pasa, *Scientific Reports* **5** (1), 8350 (2015).
27. S. P. Koenig, R. A. Doganov, L. Seixas, A. Carvalho, J. Y. Tan, K. Watanabe, T. Taniguchi, N. Yakovlev, A. H. Castro Neto and B. Özylmaz, *Nano Letters* **16** (4), 2145-2151 (2016).
28. S. W. Lee, L. Qiu, J. C. Yoon, Y. Kim, D. Li, I. Oh, G.-H. Lee, J.-W. Yoo, H.-J. Shin, F. Ding and Z. Lee, *Nano Letters* (2021).
29. Z. Lin, J. Wang, X. Guo, J. Chen, C. Xu, M. Liu, B. Liu, Y. Zhu and Y. Chai, *InfoMat* **1** (2), 242-250 (2019).
30. Y. Zheng, H. Yang, C. Han and H. Y. Mao, *Advanced Materials Interfaces* **7** (17), 2000701 (2020).
31. R. M. Feenstra, *Journal of Vacuum Science & Technology B: Microelectronics and Nanometer Structures Processing, Measurement, and Phenomena* **21** (5), 2080-2088 (2003).
32. F. Marcinowski, J. Wiebe, F. Meier, K. Hashimoto and R. Wiesendanger, *Physical Review B* **77** (11), 115318 (2008).
33. K. Teichmann, M. Wenderoth, S. Loth, R. G. Ulbrich, J. K. Garleff, A. P. Wijnheijmer and P. M. Koenraad, *Physical Review Letters* **101** (7), 076103 (2008).
34. M. Batzill, K. Katsiev, D. J. Gaspar and U. Diebold, *Physical Review B* **66** (23), 235401 (2002).
35. Y. Cui, X. Shao, S. Prada, L. Giordano, G. Pacchioni, H.-J. Freund and N. Nilius, *Physical Chemistry Chemical Physics* **16** (25), 12764-12772 (2014).
36. A. A. Khajetoorians, B. Baxevanis, C. Hübner, T. Schlenk, S. Krause, T. O. Wehling, S. Lounis, A. Lichtenstein, D. Pfannkuche, J. Wiebe and R. Wiesendanger, *Science* **339** (6115), 55 (2013).

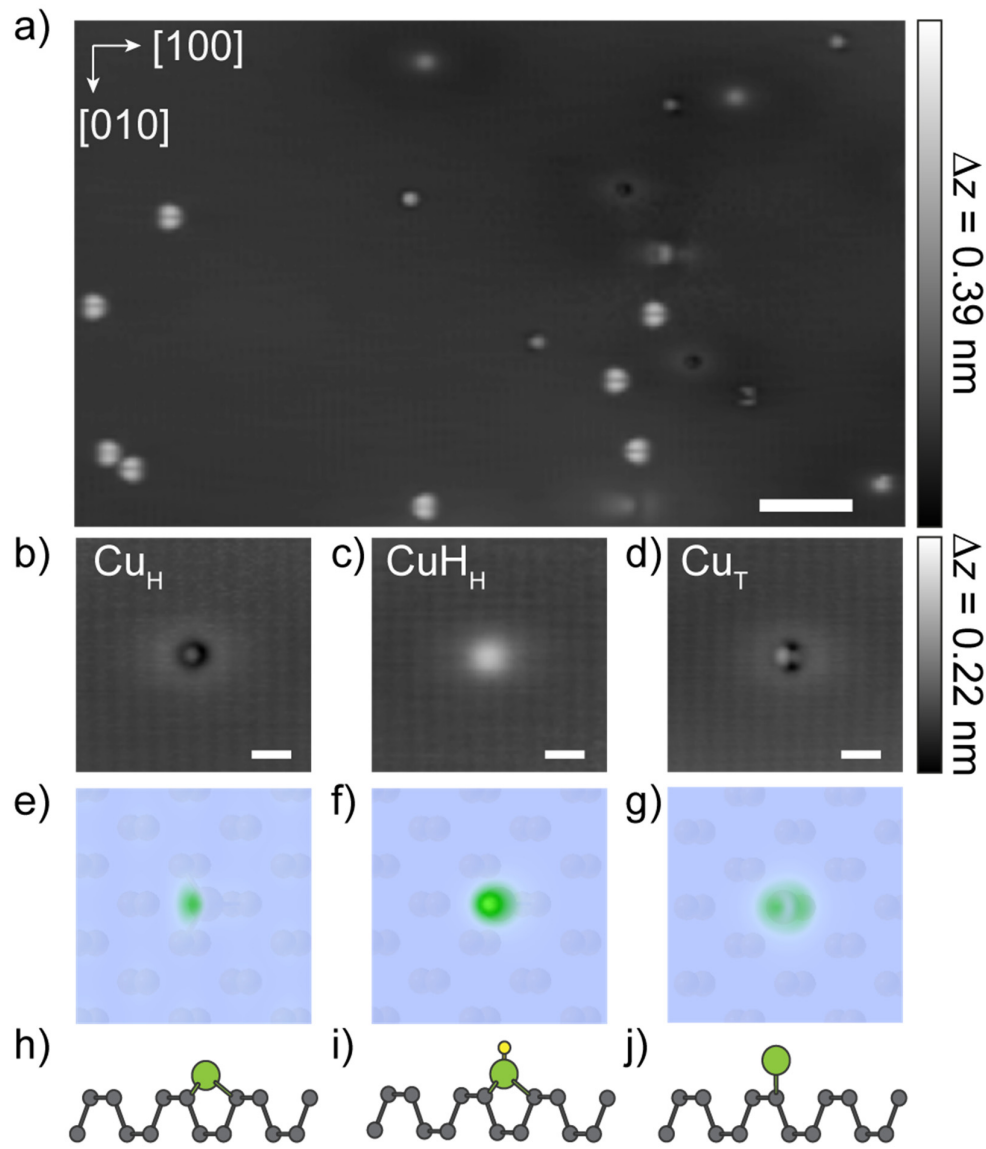


**Figure 1.** (a) STM image of individual Co and Cu atoms on the surface of BP. ( $V_S = -400$  mV,  $I_t = 20$  pA, scalebar = 5 nm). (b-d) High resolution images of the charge density of three Cu species: (b) Cu residing in a hollow site (Cu<sub>H</sub>), (c) hydrogenated Cu residing in a hollow site (CuH<sub>H</sub>) and (d) Cu residing on a top site (Cu<sub>T</sub>). ( $V_S = -400$  mV,  $I_t = 60$  pA, scalebar = 1 nm). (e-g) *Ab initio* calculations of the relaxed charge density of (e) a Cu<sub>H</sub> atom, (f) CuH<sub>H</sub> and (g) a Cu<sub>T</sub> atom. (h-j) Schematics of the relaxed atomic adsorption geometries of (h) Cu<sub>H</sub>, (i) CuH<sub>H</sub> and (j) Cu<sub>T</sub>.

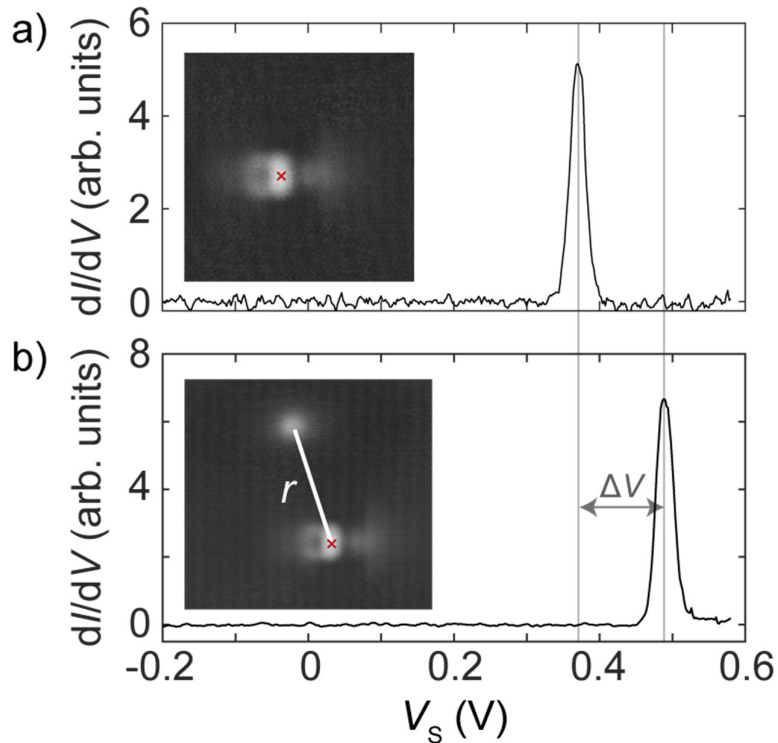


**Figure 2.** (a)  $dI/dV$  spectrum taken on an isolated Co<sub>low</sub> atom (distance to nearest Cu species  $r > 10$  nm). Inset: STM image isolated Co<sub>low</sub> atom. The red X marks the location where the  $dI/dV$  spectrum was taken. ( $V_s = -400$  mV,  $I_t = 60$  pA). (b)  $dI/dV$  spectrum taken on a Co<sub>low</sub> atom in the vicinity of CuH<sub>H</sub> (distance  $r = 3.8$  nm). The shift of the ionization peak with respect to the isolated atom is indicated by  $\Delta V$  and equals 118 mV. Inset: STM image of the Co<sub>low</sub> - CuH<sub>H</sub> pair. The red X marks the location where the  $dI/dV$  spectrum was taken. ( $V_s = -400$  mV,  $I_t = 60$  pA).

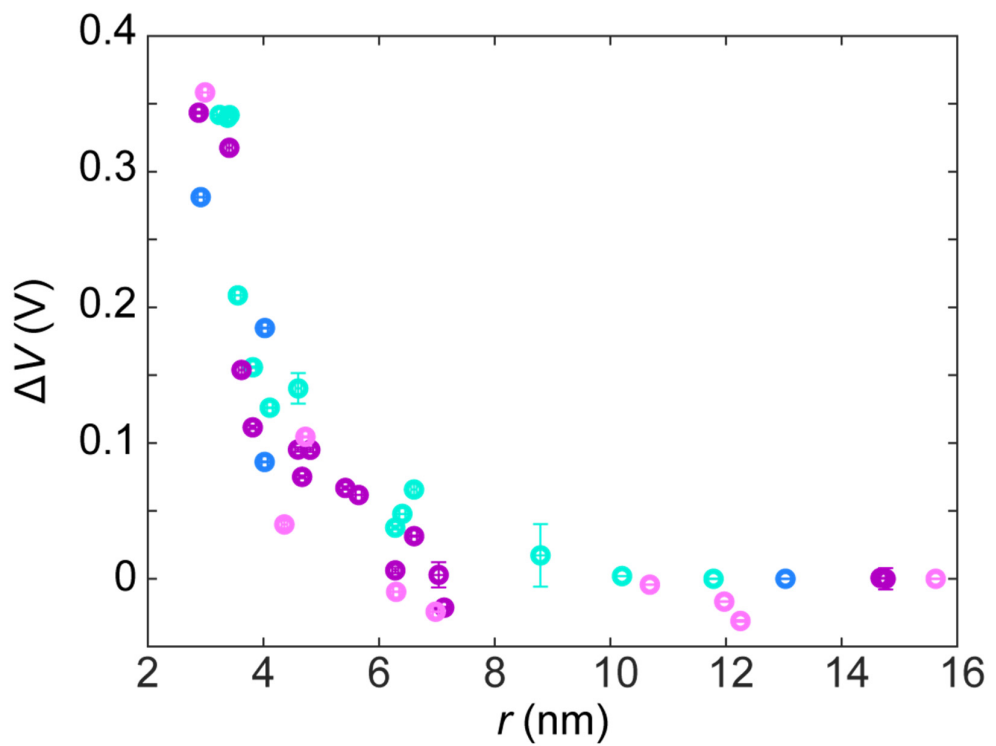


**Figure 3.** Shift of the ionization peak energy  $\Delta V$  of single  $\text{Co}_{\text{low}}$  atoms as a function of distance to a Cu species  $r$ . The shift is defined with respect to the peak energy of an isolated atom:  $\Delta V = V(r) - V(r > 10 \text{ nm})$ . Different colors represent different microtips.

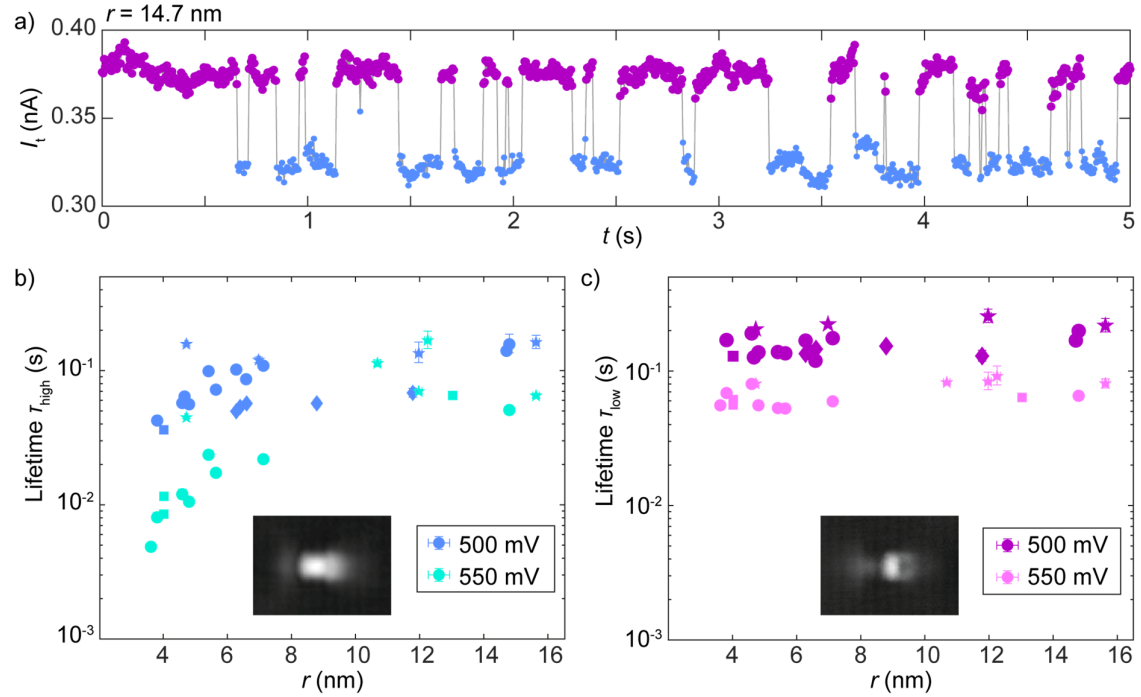


**Figure 4.** (a) Two-state telegraph noise signal of an isolated Co atom (nearest Cu donor at  $r = 14.7$  nm), with  $\text{Co}_{\text{low}}$  in purple and  $\text{Co}_{\text{high}}$  in blue. (b-c) State lifetime  $\tau$  of (b)  $\text{Co}_{\text{high}}$  and (c)  $\text{Co}_{\text{low}}$  as a function of Cu-Co distance  $r$ , for two different biases and several different microtips. Different symbols represent different microtips and different colors represent the different biases (500 mV and 550 mV). In the insets, STM images of the corresponding states  $\text{Co}_{\text{high}}$  and  $\text{Co}_{\text{low}}$  are displayed ( $V_s = -400$  mV,  $I = 60$  pA).

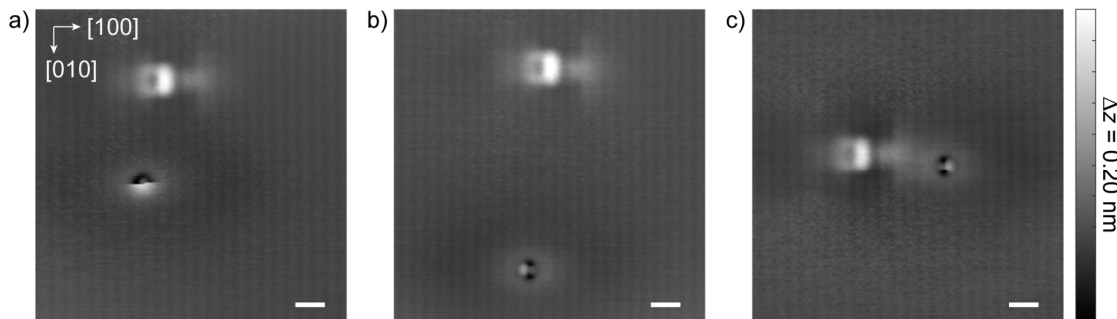
# Supplementary Information

## Table of contents

<b>Detailed information about Cu species.....</b>	<b>1</b>
<b>Copper doping of black phosphorus .....</b>	<b>1</b>
<b>Ionization peak energy of Co<sub>low</sub> atoms.....</b>	<b>4</b>
<b>Electric dipole moment of Co atoms .....</b>	<b>4</b>
<b>References.....</b>	<b>5</b>

## Detailed information about Cu species

Supplementary Figure 1 shows STM images of different pairs of a Co<sub>low</sub> atom and a Cu species. In (a), an image is displayed showing a (de)hydrogenation event of a Cu atom in the hollow site. Such an event occurs occasionally during an STM image and is in line with observations of hydrogenation of single atoms and molecules on various surfaces [1-5]. Over time, more of the Cu<sub>H</sub> atoms get hydrogenated. In Supplementary Figure 1 (b-c), a Cu<sub>T</sub> atom is shown in vicinity of a Co<sub>low</sub> atom. The Cu<sub>T</sub> atoms in both images are mirror-symmetric in the [010] direction. Similarly, mirror-symmetric species are also observed for the different Co species [6].

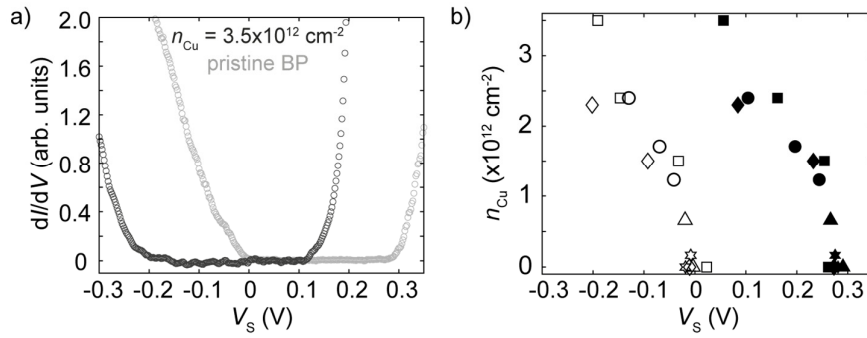


**Supplementary Figure 1.** (a) Hydrogenation event of a Cu<sub>H</sub> atom, during an STM image. (b-c) STM images of Co-Cu<sub>T</sub> pairs. The Cu<sub>T</sub> atoms are mirror-symmetric in the [010] direction. Parameters for (a-c):  $V_s = -400$  mV,  $I = 60$  pA, scalebar = 1 nm.

## Copper doping of black phosphorus

To examine the effect of Cu doping on the band structure of BP, scanning tunneling spectroscopy (STS) and density functional theory (DFT) calculations were performed. Both methods reveal that

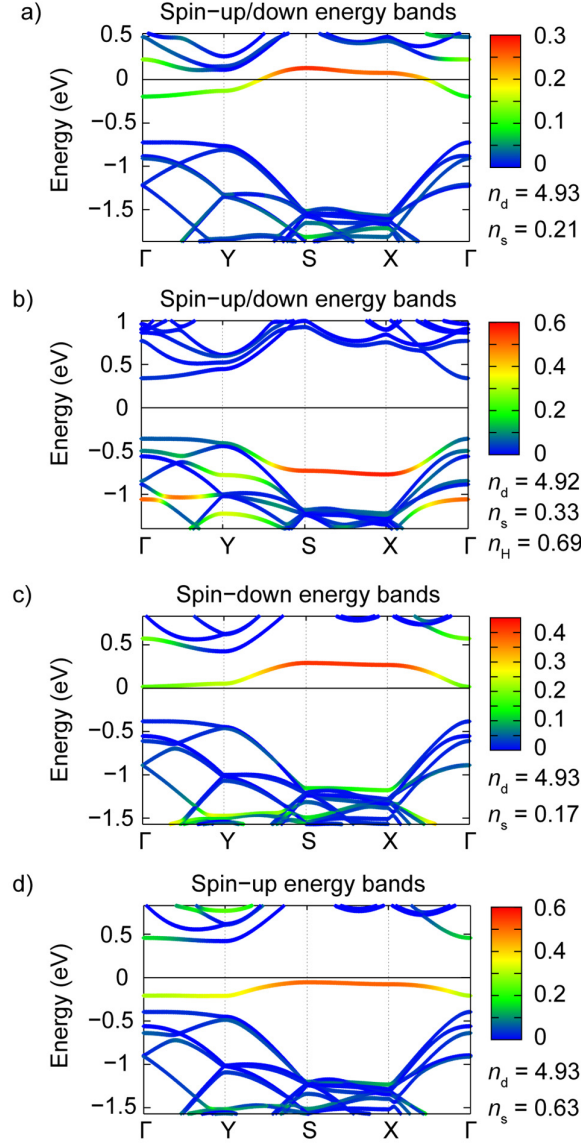
deposition of Cu on BP leads to *n*-doping, in line with literature [7-10]. Single Cu atoms were deposited on several BP samples, where after the shift in the bandgap of BP could be measured with STS at sufficiently high surface coverage. Supplementary Figure 2(a) shows  $dI/dV$  spectra of pristine BP and Cu-doped BP at a coverage of  $n_{Cu} = 3.5 \times 10^{12} \text{ cm}^{-2}$ , revealing a clear shift of the bandgap to lower energy. Supplementary Figure 2(b) shows the band edges from multiple pristine and Cu-doped BP samples, extracted using the same method as in ref [11]. For each extracted bandgap, between 25 and 160  $dI/dV$  spectra were analyzed. The extracted band edges for pristine BP are in good agreement with refs [11,12].



**Supplementary Figure 2.** (a)  $dI/dV$  spectra for pristine BP (gray) and Cu-doped BP (black) at  $n_{Cu} = 3.5 \times 10^{12} \text{ cm}^{-2}$ . (b) Valence band maxima (empty markers) and conduction band minima (filled markers) extracted from multiple  $dI/dV$  spectra taken in different spatial locations, as a function of the areal density of Cu ( $n_{Cu}$ ). Each symbol represents iterations of depositing Cu on the same BP sample. The standard error of the extracted band edges is smaller than the symbol sizes. For all spectra in (a) and (b):  $I_{\text{stabilization}} = 100 \text{ pA}$ ,  $f = 817.7 \text{ Hz}$ ,  $V_{\text{mod}} = 10 \text{ mV}$ .

Supplementary Figure 3 shows the band structure calculated within DFT for a Cu atom on BP in the hollow ( $Cu_H$ ) and top sites ( $Cu_T$ ), and in the hollow site with hydrogenation ( $CuH_H$ ). The color indicates the occupation of the 3d and 4s shell of Cu. In all cases, the phosphorus states as well as the band gap are easily distinguishable. In case of  $Cu_H$  and  $CuH_H$ , the system is nonmagnetic and the electronic bands are degenerate in spin. For  $Cu_H$  there is one band associated with Cu states at the Fermi energy, which is half-filled (Supplementary Fig. 3(a)). This band becomes fully occupied after hydrogenation (Supplementary Fig. 3(b)). The situation when Cu is adsorbed on the top site ( $Cu_T$ ) is

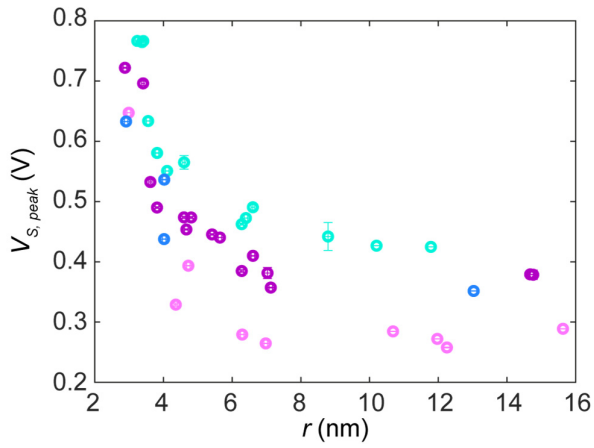
different (Supplementary Fig. 3(c-d)). In this case, the Cu states are non-spin-degenerate and Cu atoms carry a magnetic moment of  $\sim 0.5 \mu_B$ . The corresponding Cu band becomes fully occupied for the spin-up states and fully empty for the spin-down states. Non-integer magnetic moment is the result of a hybridization between copper and phosphorus states.



**Supplementary Figure 3.** Band structure of Cu-doped BP for (a)  $\text{Cu}_H$ , (b)  $\text{CuH}_H$ , (c-d)  $\text{Cu}_T$ . The color scale stands for the contribution of the different orbitals: blue bands stem exclusively from  $p$  orbitals, while red indicates a contribution from Cu orbitals. The occupation of the  $3d$  and  $4s$  shell of Cu are given below the colorbar.

## Ionization peak energy of $\text{Co}_{\text{low}}$ atoms

The ionization peak energy  $V_{\text{S,peak}}$  of single  $\text{Co}_{\text{low}}$  atoms was extracted using Gaussian fits of the peaks in the  $dV/dV$  spectra. The results for different tips are shown in Supplementary Figure 4, as a function of distance  $r$ . For each microtip, the qualitative trend is the same: there is a monotonous increase of the ionization peak energy as  $r$  decreases. Quantitatively, there is a different offset for each microtip. This can be explained by differences in the band bending condition for each microtip. To be able to compare the results from different microtips, in Figure 3 the energy difference  $\Delta V$  is shown w.r.t. an isolated Co atom ( $r > 10$ ).

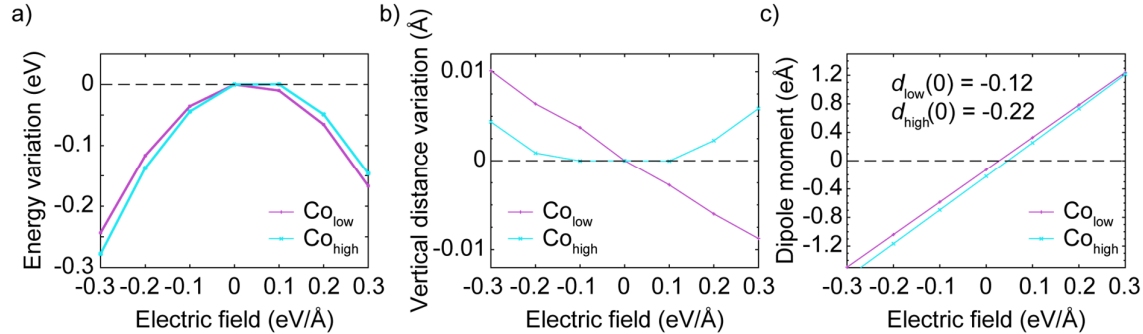


**Supplementary Figure 4.** Extracted ionization peak energy of single  $\text{Co}_{\text{low}}$  atoms as a function of distance to a Cu species  $r$ . Different colors represent different microtips and correspond to the colors in Figure 3.

## Electric dipole moment of Co atoms

Supplementary Figure 5 shows (a) energy variation, (b) vertical distance variation and (c) electric dipole moment as a function of vertical electric field calculated within DFT for low-spin and high-spin states of a Co adatom on BP. The energy variation is quadratic in electric field, and is similar for both states of the adatom. On the contrary, the vertical distance changes differently for the low- and high-spin states. While the former demonstrates a linear dependence, asymmetric with respect to the sign of electric field, the latter resembles a quadratic dependence. This behavior indicates that the vertical charge distribution is essentially different for the two states. This is further confirmed by the calculations of the electric dipole moment shown in Supplementary Fig. 5(c). Although the overall

dependence on the electric field is similar, the absolute values of the dipole moment at zero electric field are significantly different, resulting in  $-0.12$  and  $-0.22$   $e\text{\AA}$  for the low- and high-spin states, respectively.



**Supplementary Figure 5.** Ab initio calculations of (a) energy variation, (b) vertical distance variation and (c) dipole moment as a function of vertical electric field shown for low-spin and high-spin states of Co adatom on BP.

## References

- [1] A. Zhao *et al.*, *Science* **309**, 1542 (2005).
- [2] N. Baadji, S. Kuck, J. Brede, G. Hoffmann, R. Wiesendanger, and S. Sanvito, *Physical Review B* **82**, 115447 (2010).
- [3] B. W. Heinrich, G. Ahmadi, V. L. Müller, L. Braun, J. I. Pascual, and K. J. Franke, *Nano Letters* **13**, 4840 (2013).
- [4] A. A. Khajetoorians, T. Schlenk, B. Schweißinghaus, M. dos Santos Dias, M. Steinbrecher, M. Bouhassoune, S. Lounis, J. Wiebe, and R. Wiesendanger, *Physical Review Letters* **111**, 157204 (2013).
- [5] V. C. Zoldan, R. Faccio, and A. A. Pasa, *Scientific Reports* **5**, 8350 (2015).
- [6] B. Kiraly, A. N. Rudenko, W. M. J. van Weerdenburg, D. Wegner, M. I. Katsnelson, and A. A. Khajetoorians, *Nature Communications* **9**, 3904 (2018).
- [7] S. P. Koenig *et al.*, *Nano Letters* **16**, 2145 (2016).
- [8] S. W. Lee *et al.*, *Nano Letters* (2021).
- [9] Z. Lin, J. Wang, X. Guo, J. Chen, C. Xu, M. Liu, B. Liu, Y. Zhu, and Y. Chai, *InfoMat* **1**, 242 (2019).
- [10] Y. Zheng, H. Yang, C. Han, and H. Y. Mao, *Advanced Materials Interfaces* **7**, 2000701 (2020).
- [11] B. Kiraly, N. Hauptmann, A. N. Rudenko, M. I. Katsnelson, and A. A. Khajetoorians, *Nano Letters* **17**, 3607 (2017).
- [12] B. Kiraly *et al.*, *Physical Review Letters* **123**, 216403 (2019).